High-Throughput Gas Sensing Screening of Surface-Doped In_2O_3

D. Sanders and U. Simon*

RWTH Aachen University, Institute of Inorganic Chemistry, D-52056 Aachen, Germany

Received April 6, 2006

The effect of various surface doping elements on the electrical and gas sensing properties of indium(III) oxide thick films sensors was investigated by means of high-throughput impedance spectroscopy (HTIS). Some doping elements lead to changes in both the conductivity in air as well as in the gas sensing properties towards oxidizing (NO_2, NO) and reducing (H_2, CO, propene) gases. Correlations between the sensing and the electrical properties in reference atmosphere indicate that the effect of the doping elements can be ascribed to an influence on the oxidation state of the metal oxide surface rather that to an interaction with the respective testing gases. An equation for the description of the temperature-dependent conductivity in air and nitrogen is proposed to describe the oxidation state of the metal oxide surface taking into account sorption of oxygen. Furthermore, a model associating the sensing properties and the oxidation state of the surface layer of the metal oxide based on oxygen spillover from doping element particles to the metal oxide surface is introduced.

Introduction

Indium(III) oxide is an *n*-type semiconductor known for its resistive gas sensing properties. It is described as material showing pronounced rise in electrical resistivity toward exposure to small concentrations of oxidizing gases (NO_2,[1−6] O_3,[7−9] NO,[10] SO_2,[3] Cl_2[2]) as well as reducing gases (H_2,[11] CO[2−8,12]). Besides doping elements or additives, the crystallinity and thickness of the respective base material including details of the coating preparation, geometry as well as the materials used for the test substrates, aging and preconditioning procedures, and the testing conditions show pronounced influence on the sensitivity determined in a sensor material characterization.[13] Thus, the investigation of the influence of one specific parameter demands for the discrimination of effects of unknown origin. The usual way is to keep most parameters constant by ensuring identical sample procedure and processing while selectively varying only one parameter under investigation. Due to the limitation in sample throughput, such an investigation is often restricted to few samples, which leads on the one hand to a preselection of *promising* variations disregarding possible alternative material compositions. On the other hand, the limited amount of data reduces statistical reliability of systematic evaluations.

The use of high-throughput experimentation (HTE) techniques can cope with both limitations. HTE accelerates material synthesis and characterization, enabling the investigation of a multiplicity of materials compared to the "one at a time" strategy. Hence the high throughput is usually achieved by using sample plates containing multiple materials under test; accompanied with a rise in samples per investigation, maximal homogeneity of sample preparation and handling can be achieved. In this context we reported on the design of 8 × 8 multielectrode arrays for high throughput screening of electrical properties of solid-state samples[14] and the development of an appropriate high throughput impedance spectroscopy system (HTIS) for automated screening for gas sensitive properties.[15] We also present the first results for a materials library containing variously doped WO_3[16] as well as La-doped $CoTiO_3$.[17]

In continuation of these developments, this paper reports the HTIS screening of the gas sensitivity (H_2, CO, NO, NO_2, propene) for an In_2O_3-based material library together with the development of a model to describe the structure−property relations. Diversity is achieved by various surface doping elements, while the base material In_2O_3 originates form a single synthesis. In addition to noticeable effects found for some doping elements, a systematic effect discovered by means of data mining in the screening dataset is presented and discussed based on additional measurements of the temperature-dependent conductivity in air and in nitrogen. Furthermore a model for the effect of doping elements is discussed.

Experimental Section

Sample Preparation and Library Design. The base material was obtained from pyrolysis of indium(III) acetate (350 °C, 6h), resulting in spherical In_2O_3 particles of cubic symmetry (206)[18] with diameters between 40 and 150 nm (X-ray diffraction pattern and scanning electron microscopy shown in Figure 1). The oxide was dispersed by mixing in a mortar with water. The coating of the multielectrode arrays (substrate: Al_2O_3; electrodes: interdigital type; electrode width: ∼125 μm; electrode distance: ∼125 μm; sample area: ∼2 mm × 3.5 mm; for further details see ref 14). By applying each 4 μL of aqueous suspension (0.133 wt %) using an Eppendorf pipet uniform thick films resulted after drying under atmospheric conditions. The mean film thickness was 300 μm.

Surface doping elements where introduced by wetting impregnation of aqueous (except $Ga(C_5H_7O_2)_3$ in toluene)

* Corresponding author. Tel.: +49-241-8094644. Fax: +49-241-8099003. E-mail: ulrich.simon@ac.rwth-aachen.de.

10.1021/cc060044p CCC: $37.00
Published on Web 12/15/2006

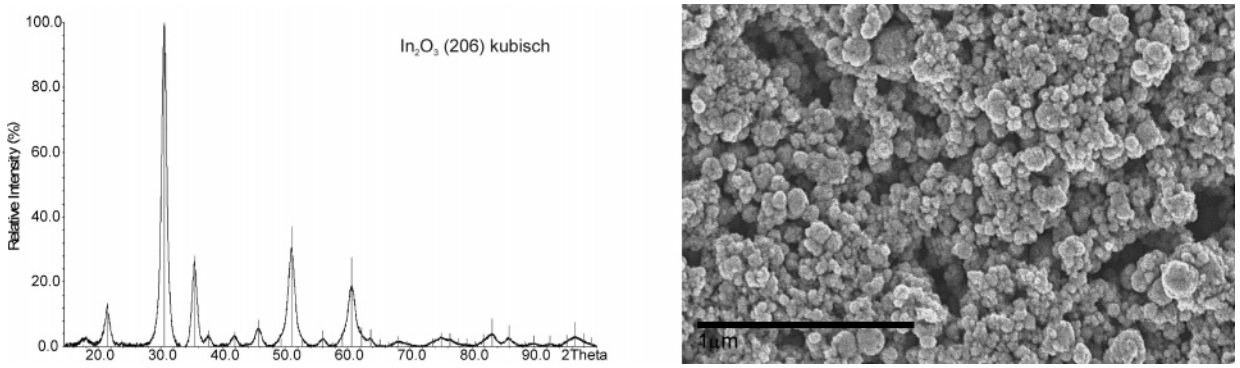

Figure 1. X-ray diffraction pattern and scanning electron micrograph picture of In_2O_3.

solutions of nitrates, acetates, acetylacetonates, element acids, and $HAuCl_4$, followed by calcination (400 °C, 5 h) (Figure 8 gives an overview of the introduced doping elements). The library consists of three sample plates (sample coated multielectrode arrays), focusing on reproducibility (plate RA6350, which is coated four times with 16 identical doping), high doping element diversity (plate RA6418), and variation of doping concentration of elements that showed influence on the sensing properties when screening plate RA6418 (plate RA6423). The concentration of the doping in atomic percentage was calculated in relation to indium.

Screening Flow for Gas Sensing Properties. The gas sensing properties of the individual samples were determined by means of HTIS. For further details on HTIS, we refer to ref 15. As a standardized screening sequence, the materials were electrically characterized by complex impedance spectroscopy (impedance analyzer: Agilent 4192A: $10-10^7$Hz, amplitude 0.1 V rms) in synthetic air with a relative humidity of 45% (25 °C) and. serving as reference and carrier gas, 25 ppmH_2 , 50 ppm CO, 5 ppm NO, 5 ppm NO_2, and 25 ppm propene at temperatures between 400 and 250 °C in 50° steps. After arriving at a respective temperature, the materials were conditioned for 90 min in reference atmosphere. The preliminary gas run was 15 min in each case. All testing gas measurements were followed by a measurement in reference atmosphere to investigate the reversibility of the materials response.

The sensor responses (i.e., the relative sensitivities S_Δ) were calculated using the following equations:

$$S_\Delta = +\frac{R_0 - R_{TEST}}{R_0} \text{ for } R_0 > R_{TEST};$$

$$S_\Delta = -\frac{R_{TEST} - R_0}{R_{TEST}} \text{ for } R_{TEST} > R_0$$

R_0 is the materials resistance from the first measurement at each temperature. In contrast to the commonly used sensitivity S as quotient of the resistances in air and under testing gas, respectively, the equations result in values between -1 and 1 simplifying automated data mining and visualization, which is vital for high-throughput investigations. The algebraic sign characterizes the gas as reducing for positive and oxidizing for negative values, respectively.

Temperature-Dependent Conductivity. For a detailed analysis of the temperature dependence of the conductivity, undoped and 0.1 atom % Rh-doped In_2O_3 were deposited on single sensor substrates analogous to the procedure described in sample preparation. The substrates exhibit a heating element (Pt) on the backside for direct heating. The sensors were conditioned at 500 °C for approximately 30 min in each atmosphere. The samples dc-conductivity was measured in a gas flow of synthetic air (20% O_2:80% N_2) and nitrogen, respectively, using a Sourcemeter Keithley 2400 at 1 V during the cooling between 500 and 40 °C. Prior to each measurement, the temperature was kept constant for 1 min.

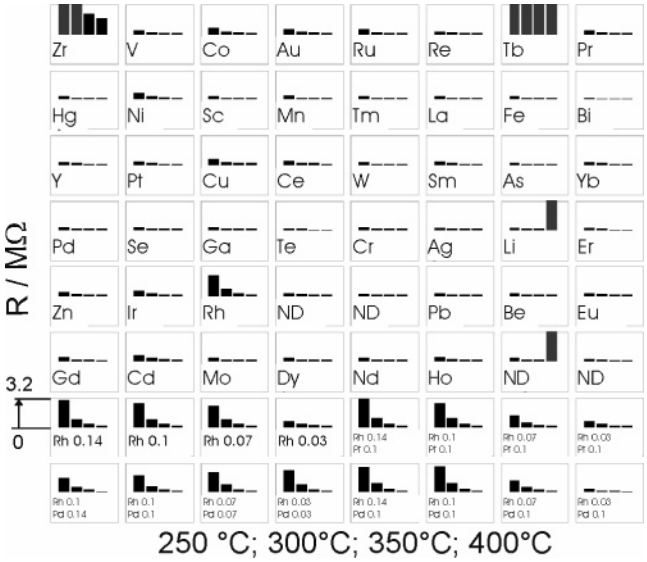

Figure 2. Resistances of the samples on plate RA6418 in humid air in the temperature range from 250 to 400 °C. Gray bars stand for values exceeding the scale. The indices denote the doping element (concentration 0.1 atom % if not denoted otherwise). ND refers to undoped samples.

Results and Discussions

General Electrical Properties. The electrical properties of all sample positions could be described with the impedance function of a parallel *R*;*C*- circuit equivalent. By means of automated data fitting[15] *R*;*C*- circuit equivalents are adjusted to the measured impedance spectra to determine the resistance R and the capacitance value C_{IDK}, respectively. The capacity C_{IDK} is given by the geometric capacity of the measuring electrodes with the sample acting as a dielectric, while R represents the ohmic resistance of the sample.

Figure 2 plots each samples resistance for sample plate RA6418 in humid air as a bar diagram at the respective

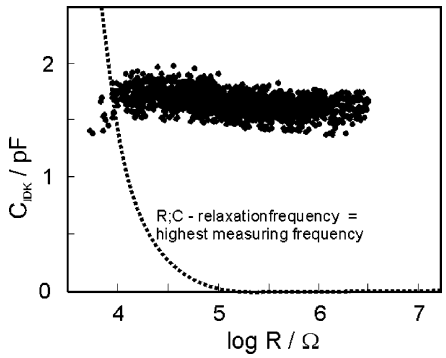

Figure 3. Data fit results plotted as C_{IDK} vs log R for sample plate RA6418 including all temperatures as well as all testing gas. The dotted line indicates the highest measuring frequency, expressed as the increase of the product of R and C (i.e., the relaxation time).

measuring temperature in the pattern of the samples position on the plate. To refer to individual samples, the position is expressed by a <x|y> notation, in which x and y corresponde to rows and columns, respectively.

All samples show decreasing resistances with rising temperature, as expected for a semiconductor. For the Rh-doping, a clear trend can be observed (e.g., <1|7> – <4|7>). Obvious high resistances appear in Rh <3|4> (temperatures <350 °C) and Zr <1|1> doped In_2O_3. The latter was reevaluated and can be explained by a faulty electrode structure. Residual exceptional high resistances (Tb doping <7|1>, Li <7|4> and ND <7|6> at 400 °C) can be assigned to defective contacted electrode positions. The effect of Rh is also apparent for the samples with mixed surface doping, where Rh is applied in a concentration gradient.

Figure 3 reflects the samples capacitance and resistance for plate RA6418 at all investigated temperatures and for all testing gases. While temperature as well as testing gas show influence on in the materials resistance, no significant change in the capacitances is found. The variation of the capacitance values in Figure 3 can be ascribed to varying film thickness and density, respectively. Only a minor general rise of C_{IDK} toward smaller resistances can be observed. Therefore, it can be assumed that the testing gases show no significant influence on the material's permittivity. Note that measurements with relaxation frequencies above the highest measurement frequency apparently show decreased capacitance values. Here data fitting cannot extrapolate the samples capacity.

We do not see any hints on an intra-particle charge current relaxation. This should be dependent on the extension of the Schottky barriers at the inter-particle contact, according to the general model of the gas sensitivity semiconducting oxides.[19,20] This is in accordance with the observations reported by Korotcenov et al. that the resistance of polycrystalline In_2O_3 films is independent of the grain size, indicating that either the height of potential barriers between oxide particles is low or that the concentration of ionized donors at the surface of the particles is high.[11]

Sensing Properties. The homogeneity and comparability of the samples was studied by determining the sensitivity of each 16 identically doped samples of three doped and the undoped positions. Figure 4 shows the materials response toward testing gases as a mean value of S_Δ with the standard deviation, plotted as error bars.

In general the minor standard deviations correspond to a uniform and reproducible response of the respective materials. As an exception for CO significant variations are observed. Detailed analysis indicated that CO was catalytically converted in the presence of oxygen due to the catalytic activity of some materials on the sample plate, resulting in a concentration gradient from center to edge positions of the plate. Due to this fact we pass on further exacting discussion of CO sensitivities.

Undoped In_2O_3 responds highly sensitive toward 25 ppm H_2 and propene by means of a resistance decrease, whereas 5 ppm NO and NO_2 cause a distinct increase in the materials resistance for low temperatures. Doping with Pd (0.1%at) enhances the sensitivity toward reducing gases up to 350 °C, while at 400 °C decreased values for S_Δ are found. The most pronounced effect on the sensitivity results from Rh doping. The NO_2 sensitivity is almost eliminated. The character of NO changes from oxidizing (increase of resistivity, i.e., $S_\Delta < 0$) to reducing (decrease of resistivity, i.e., $S_\Delta > 0$) at low temperatures. Toward H_2 and propene a decrease of sensitivity is obvious with rising temperature. At the same time Rh-doped In_2O_3 shows the highest H_2 sensitivities observed (250 °C).

Figure 5 exemplarily shows plots of individual samples sensitivity for plate RA6418 as bar diagrams on the testing gas run for 250 and 350 °C in the pattern of the samples position on the plate.

In general, all materials show high sensitivity toward the reducing gases H_2 (first bar) and propene (ninth bar). For CO (third bar) increased sensitivity can be found for Rh-doping <3|5> and Rh containing samples at 250 °C as well as for the doping elements Pd <1|4>, Pt <2|3>, Ag <6|4>, and Au <1|4>. Typical response to the oxidizing gases NO (fifth bar) and NO_2 (seventh bar) is an increase of the resistance. Here the measurements in synthetic air following the gas admixture show irreversible changes in resistance in the investigated time scale (15 min) at 250 °C. This effect vanishes at higher temperatures, where full recovery is observed. As an obvious exception Ir <2|5>- and Rh-doped In_2O_3 responds toward NO by a resistance decrease, whereas for Ir an increased resistance in the reversibility measurements can be observed. Rh 0.1 atom % doped In_2O_3 reversibly responds to NO by decreased resistance (250 °C) showing no cross sensitivity toward NO_2. Ru <5|1> and Ce <4|3> influence the sensing properties of In_2O_3 by decreasing the sensitivity toward NO and NO_2. The elements, that show an effect on the gas sensing properties of In_2O_3, were investigated in dependence of the element concentration (Au, Ce, Ir, Pd, Pt, Rh, Ru; Ag was left out due to similar responses compared to Pt, Pd and Au, instead Cr was investigated). Figure 6 plots the sensitivities on the element concentration of the respective doping element.

Rh, Ir, Ru, and Ce can be grouped due to similar effects on the gas sensing properties, sequenced here after the descending intensity of the effect. With rising element concentration, the oxidizing character of NO and NO_2 is converted toward reducing and suppressed, respectively. At

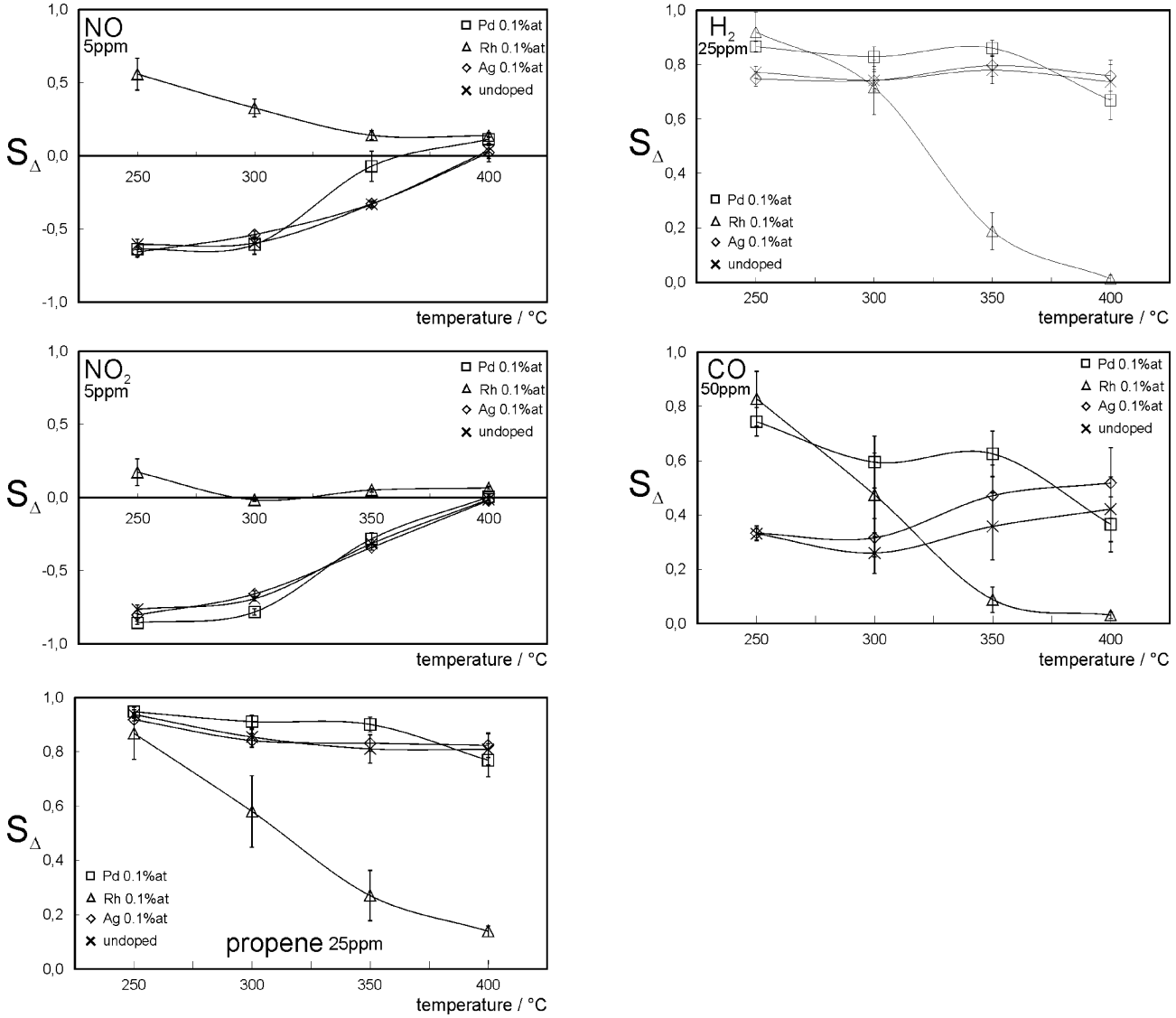

Figure 4. Mean values of the relative sensitivities of each 16 Ag-, Rh-, and Pd-doped and undoped In_2O_3 samples. The error bars represent the standard deviation deduced from identically doped samples (plate RA6350).

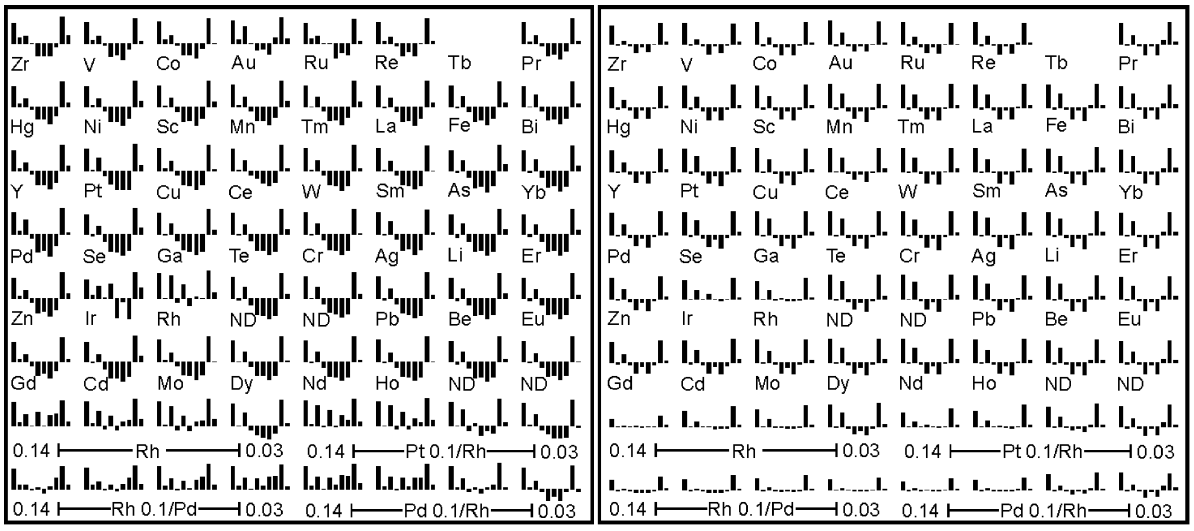

Figure 5. Relative sensitivities S_Δ of sample plate RA6418 at 250 °C (left) and 350 °C (right) on the testing gas run (H_2, air, CO, air, NO, air, NO_2, air, propene, air). The *y*-scaling is −1:1. The indices denote the doping element (concentration 0.1 atom % if not denoted otherwise). ND stands for undoped. Note that the Tb-doped sample (row 1, column 7) was not measurable due to a defect electrode structure.

the same time the response toward the reducing gases propene and H_2 is suppressed (for Rh only at $T > 250$ °C). Pt doping slightly reduces the sensitivity, with the exception of propene at 250 °C. Doping with Cr, Au and Pd typically

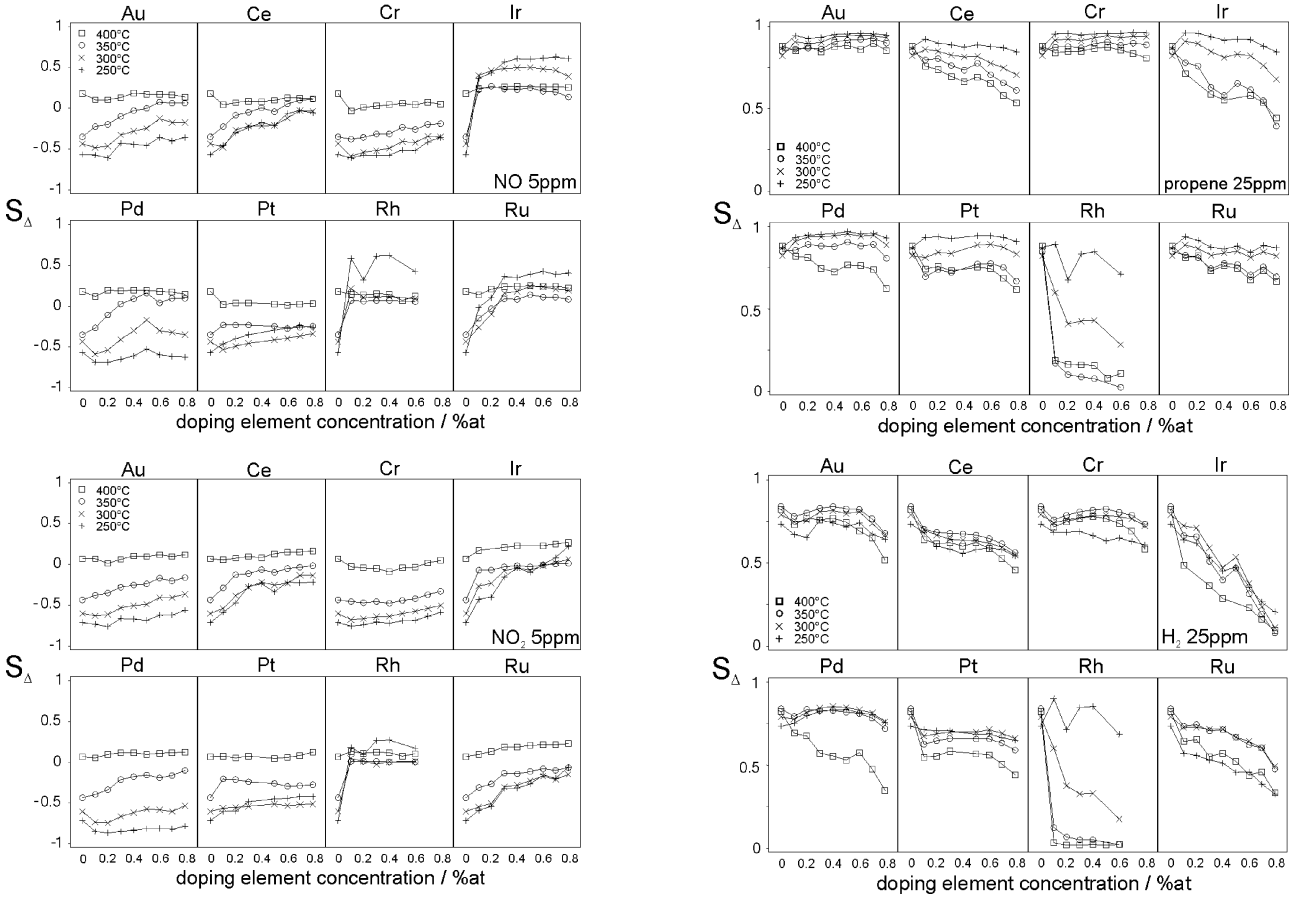

Figure 6. Dependence of the sensitivities on the concentration of doping elements (plate RA6423).

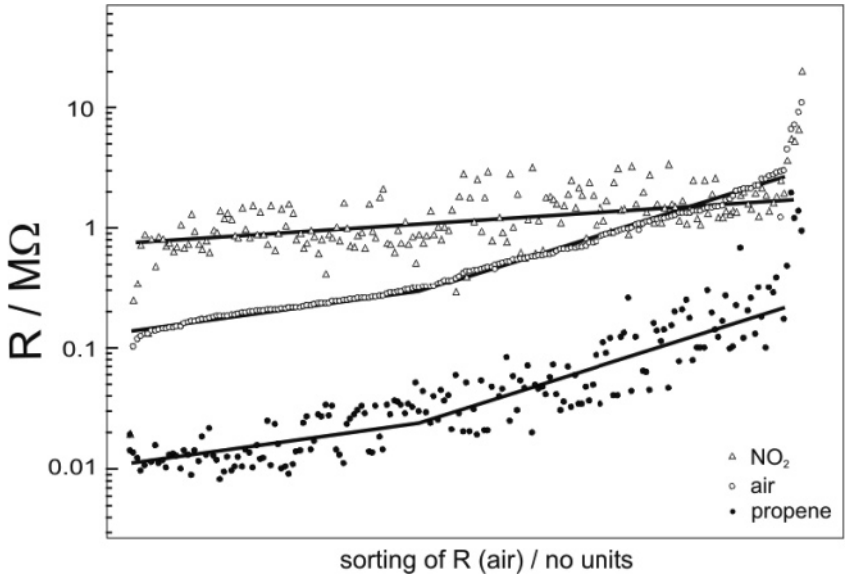

Figure 7. Plot of the resistances of the In_2O_3 library in humid air sorted according to increasing values together with the corresponding resistances in 5 ppm NO_2 and 25 ppm propene at 250 °C.

enhances S_Δ for propene. For Pd and $T = 400$ °C reduced values for S_Δ can be observed for propene and H_2.

Correlation between Sensing and Electrical Properties. By means of visual data mining the data set generated by the gas sensing screening of the material library was investigated. The aim was to find outstanding sensing properties of individual samples and to search for general correlations or patterns between sensitivities and further sample properties besides the chemical composition, respectively. A correlation of the sensitivity and the electrical properties in the reference atmosphere (humid air) was discovered.

Figure 7 shows the samples resistances in humid air, 5 ppm NO_2, and 25 ppm propene. The data for each sample are plotted on the ascending sorted resistance in humid air in order to visualize their correlation.

Two slopes can be observed for the resistance values in humid air. A small slope is found for small resistances ($R =$

Ea / eV	0.1 – 0.15	0.15 – 0.2	0.2 – 0.25	0.25 – 0.3	0.3 – 0.35	0.35 – 0.4	0.4 – 0.45	0.45 – 0.5	0.5 – 0.55	0.55 – 0.6	0.6 – 0.65	0.65 – 0.7	0.7 – 0.75	0.75 – 0.8	0.8 – 0.85
		ND													
		Yb0,1													
		Y0,1													
		W0,1													
		V0,1													
		Tm0,1													
		Sm0,1													
		Se0,1	Zn0,1												
		Sc0,1	Pt0,1												
		Re0,1	Pr0,1												
		Pd0,2	Pd0,1		Rh0,03 Pd0,1	Ru0,1									
		Pd0,1	Ni0,1	Zr0,1	Pt0,3	Rh0,03 Pt0,1									
		Pb0,1	Nd0,1	Pd0,8	Pt0,2	Rh0,03									
		Mo0,1	Mn0,1	Pd0,3	Pt0,1	Pt0,8	Pt0,7			Ru0,8	Rh0,2				
		Ga0,1	La0,1	Li0,1	Pd0,7	Pt0,5	Pt0,6			Ru0,7	Rh0,1 Pd0,14				
		Fe0,1	Ho0,1	H_2O	Pd0,6	Pd0,5	Cr0,7			Ru0,6	Rh0,1 Pd0,1				
		Er0,1	Hg0,1	Cr0,2	Pd0,4	Cr0,6	Ce0,6			Ru0,5	Ir0,7		Rh0,1 Pt0,1		
		Dy0,1	Gd0,1	Cr0,1	Cr0,4	Cr0,5	Ce0,5	Ru0,2		Ru0,4	Ir0,6		Rh0,1 Pd0,1		
		Cr0,1	Eu0,1	Ce0,1	Cr0,3	Au0,8	Ce0,4	Ru0,1		Ru0,3	Ir0,4	Rh0,1	Rh0,1 Pd0,07	Rh0,6	
	Te0,1	Bi0,1	H_2O	Au0,2	Co0,1	Au0,7	Ce0,3	Cr0,8		Rh0,07 Pt0,1	Ir0,3	Rh0,1	Rh0,1 Pd0,03	Rh0,14 Pd0,1	
	In0,1	Be0,1	Cu0,1	Au0,1	Ce0,1	Au0,5	Ce0,2	Ce0,8		Rh0,07 Pd0,1	Ir0,1	Rh0,07	Rh0,14 Pt0,1	Rh0,14	Rh0,4
	Ag0,1	As0,1	Cd0,1	Au0,1	Au0,3	Au0,4	Au0,6	Ce0,7		Ir0,8	Ir0,1	Ir0,2	Ir0,5	Rh0,1	Rh0,3

Figure 8. Compilation of the doping elements (element|concentration/atom %; ND denotes undoped) after activation energy ranges of the conductivity in reference atmosphere E_A.

(0.2 ± 0.1) MΩ). Since the resistances for undoped In_2O_3 (between 0.15 and 0.27 MΩ) can be found in this range, we assume no significant effect of the surface doping on the resistance here. The scattering of values is ascribed to variations in the thickness and the density of the samples. For higher resistances ($R > 3$ MΩ) a rise in the slope can be observed for the resistances in humid air. The corresponding samples contain the doping elements Zr, Rh, and Rh in combination with other doping elements: Ce, Cr, Pt, Ru, Au, Ir, Co, and Ni. Higher concentrations of the respective doping element typically increase the resistance. The slopes of the resistance values in air and under admixture of 25 ppm propene (250 °C) follow almost the same trend showing an offset of a factor of ~10, which corresponds to the overall high sensitivity toward propene at 250 °C.

In the presence of the oxidizing gas NO_2 a fare smaller variation of resistances is found. The general trend of the smallest resistance values can be described approximately linear with a small slope compared to the slopes observed for the resistances in air and propene, respectively. Therefore both resistances in air and in the presence of NO_2 approach at high resistance values (approximately 1 MΩ), what corresponds to a diminishing sensitivity. It is clearly visible that the sensitivity toward the oxidizing gas NO_2 can be derived from the resistance in air rather than by the resistance in the testing gas atmosphere. High sensitivities can be observed for small resistances in the reference atmosphere. Thus the sensitivities toward NO_2 can be predicted simply based on the resistances in the reference atmosphere, whereby high resistances result in low sensitivities and vice versa. A similar effect can be observed for the testing gas NO.

As a further result of data mining a correlation between the sensitivities to testing gases and the temperature dependence of the electrical conductivity in air, expressed by the activation energy E_A was discovered. The values of E_A were calculated by means of the Arrhenius equation using each the first resistance R in synthetic air measured at temperatures of 300, 350, and 400 °C ($E_{A(300°C-400°C)}$). Note that the values of E_A do not necessarily represent the thermal activation of a distinct electrical process since the temperatures used for the calculation where selected arbitrarily. Figure 8 compiles the investigated samples in order to trend their respective activation energies.

While most values of $E_{A(300°C-400°C)}$ are arranged ± 0.15 eV relative to undoped In_2O_3, Ce, Au, Pt, Pd, Ru, Ir, and Rh doping results in a pronounced increase of E_A. As a general trend, rising dopant concentration increases the values of $E_{A(300°C-400°C)}$. Figure 9 plots the relative sensitivities S_Δ on $E_{A(300°C-400°C)}$. For clearness only the temperatures 250 and 400 °C are displayed.

The relative sensitivities toward NO and NO_2 show an obvious correlation by increasing values for S_Δ with increasing $E_{A(300°C-400°C)}$ at 250 °C. Compared to NO_2, S_Δ for NO is slightly shifted toward reducing character. At $E_A \sim 0.5$ eV (NO) and $E_A \sim 0.7$ eV (NO_2), the sensitivities turn from oxidizing to reducing character. This correlation diminishes with rising temperature, presumably mainly due to the general decrease of sensitivity toward NO and NO_2 as compared to the other gases. Therefore at 400 °C no trend of the sensitivity can be observed for NO and NO_2. For propene and H_2 a trend toward decreasing sensitivities with

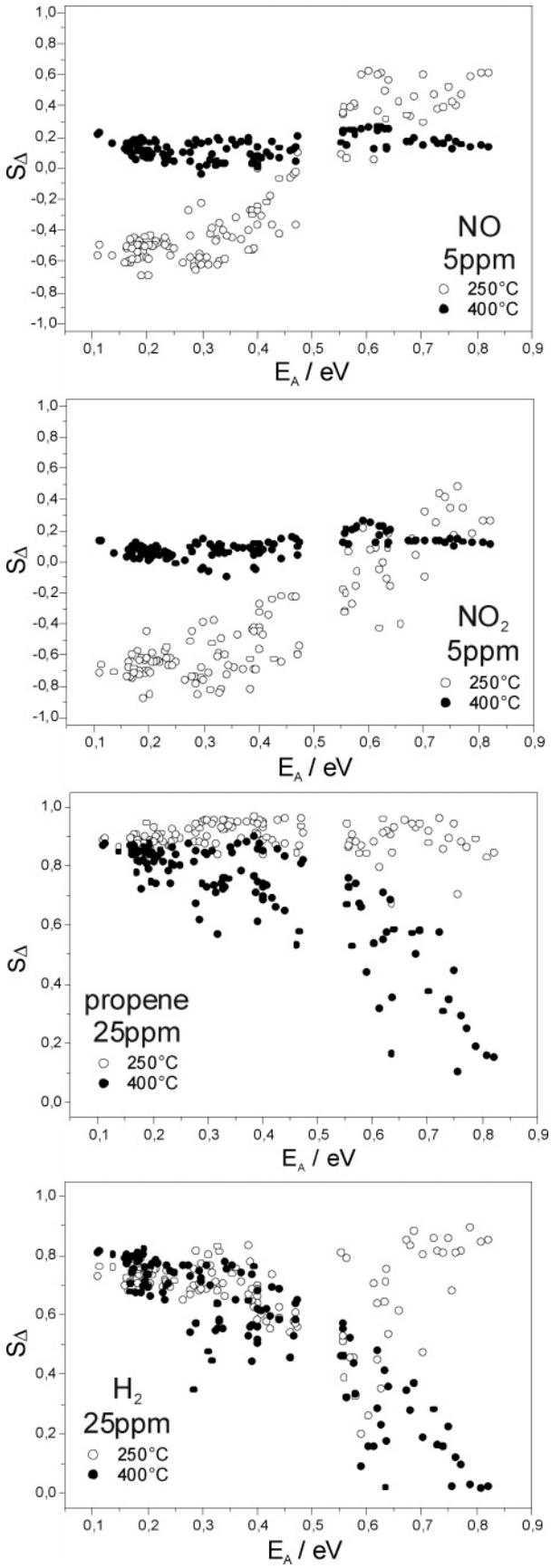

Figure 9. Relative sensitivities S_Δ vs activation energies $E_{A(300°C-400°C)}$ of the conductivity in humid air.

rising values of $E_{A(300°C-400°C)}$ can be observed for elevated temperatures.

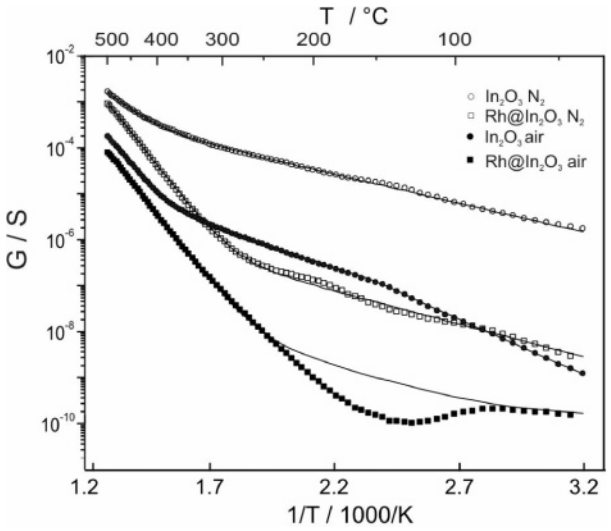

Figure 10. Arrhenius plot in synthetic air and nitrogen for undoped and Rh 0.1 atom % doped In_2O_3. The solid line represents the curve fitting based on eq 2.

Both correlations indicate that the sensitivity depends on the electrical properties in the reference atmosphere rather than on electrical properties in the presence of testing gas. This finding is most pronounced for oxidizing gases at low temperatures and for reducing gases at elevated temperatures. It can be assumed that the doping primarily affects the sensitivity by changing the electrical properties in the reference atmosphere.

Temperature Dependence of the Resistance. For a detailed analysis of the temperature-dependent resistance R and of the conductance $G = 1/R$, respectively, measurements of an undoped and Rh 0.1 atom % doped In_2O_3 single sensors were performed. The doping element Rh was chosen due to its large influence on the gas sensing properties observed in the screening and its pronounced effect on the activation energy of the conductivity in air, respectively. Besides measurements in air representing reference conditions the effect of a nitrogen atmosphere was investigated in order to model the condition in a reducing (oxygen free) gas atmosphere. Figure 10 shows the plot of the materials' conductance G on the reciprocal temperature (Arrhenius plot). The run of the temperature-dependent conductances were described by an equation based on the superposition of intrinsic conductivity of the semiconducting metal oxide and an impurity conductivity due to the partially reduced surface.

The electronic conductance is given by

$$G = e \cdot \mu \cdot n \cdot (d/A) \qquad (1)$$

where e is the elementary charge, μ is the electron mobility, n is the electron density in the conduction band, and d/A is a factor describing the geometry of the measuring samples. Disregarding the electron mobility μ, the temperature dependence of the conductance is directly proportional to the temperature dependence of the electron density in the conduction band. Based on eq 1 and the following equation,

Table 1. Parameters for the Curve Fitting (Figure 10; eq 2)

	N_D[a]	$E_C - E_D$/eV	N_V[a]	E_g/eV	$[O_2]_0$[a]	$E_{A,O2}$/eV
In_2O_3 air	$9.4 \cdot 10^{15}$	0.69	$1.3 \cdot 10^{24}$	2.79	$3.1 \cdot 10^{17}$	0.16
In_2O_3 N_2	$1.0 \cdot 10^{17}$	0.50	$4.3 \cdot 10^{22}$	2.08		
Rh|In_2O_3 air	$6.2 \cdot 10^{13}$	0.69	$4.1 \cdot 10^{23}$	2.75		
Rh|In_2O_3 N_2	$7.5 \cdot 10^{14}$	0.58	$4.9 \cdot 10^{24}$	2.75		

[a] Dimensionless (−) values.

the conductances shown in Figure 10 were adjusted disregarding the electron mobility and the geometry ($\mu = d/A = 1$):

$$n(T) = n_0 + [N_D - {}^1/_2[O_2](T)] \exp\left(\frac{-(E_C - E_D)}{2kT}\right) + N_V \exp\left(\frac{-E_g}{2kT}\right) \quad (2)$$

$$[O_2](T) = [O_2]_0 \exp\left(\frac{-E_{A,O2}}{kT}\right), T \leq 150\ ^\circ\mathrm{C} \quad (3)$$

$$[O_2](T) = 0; T > 150\ ^\circ C \quad (4)$$

E_C is the energy of the conduction band edge. N_D and E_D are the relative donor density and energy, respectively. N_V is the relative density of states in the valence band, E_g represents the electrical band gap. n_0 represents an, as a first approximation, temperature-independent charge carrier density. A number of $n_0 = 8.1 \cdot 10^8$ was determined by curve fitting and therefore was assumed to be constant for all measurements. The inclusion of n_0 fits the temperature-independent part for the Rh-doped materials in air at temperatures below 80 °C. The term comprising N_D and E_D represents charge carriers resulting from a partially reduced surface, which is acting similar to an impurity in doped semiconductors by providing electrons for the conductivity processes. For undoped In_2O_3 and temperatures below 150 °C, a term describing the sorption of oxygen $[O_2](T)$ has to be taken into account. O_2 effects the redox state of the surface, the adsorption of one oxygen molecule finally leads to the oxidation of two reduced surface states. At elevated temperatures a second conductivity process leads to a rapid increase of conductivity and hence shows a higher activation energy, which is almost identical for all samples and measuring conditions, respectively. This process is related to the intrinsic semiconductivity of indium oxide.[21,22] Table 1 gives the values for the fitting curves plotted in Figure 10. Due to the estimations ($\mu = d/A = 1$) made, the values of N_D, N_V, and $[O_2]_0$ are dimensionless and hence can only be used to compare among each other.

The values of E_g are in good agreement with the indirect band gap reported for In_2O_3 (E_g single-crystal 2.62 eV[21]; E_g polycrystalline material 2.7 eV[22]). The smaller value determined for undoped In_2O_3 in N_2 may be caused by the fact that the transition toward intrinsic conductance starts to appear at the highest temperatures measured.

The calculated curves fit very well with the measured conductivities. Only for the Rh doped In_2O_3 in air a deviation is obvious between 100 and 250 °C. The applied model assumes that undoped In_2O_3 desorbs oxygen at temperatures up to 150 °C in air. The process exhibits an activation energy of $E_{A,O2} = 0.16$ eV. As a result the surface is partially reduced, which leads to an enhanced concentration of charge carries accompanied with increased conductivity. For Rh doped oxide no change in conductivity can be observed which would indicate a desorption of O_2. The concentration of charge carriers is estimated to be 150 times smaller as compared to the undoped oxide. This leads us to the conclusion that Rh effectively stabilizes the surface oxygen layer. The intrinsic conductivity process is not affected by the doping with rhodium.

Conclusions

The introduction of some surface doping elements drastically change both the temperature-dependent conductivity in air and the gas sensing properties toward oxidizing and reducing gases. Most pronounced effects can be observed for rhodium, iridium, ruthenium and cerium. For undoped indium oxide a thermally induced desorption of oxygen is deduced from temperature-dependent conductivity in air below 150 °C, which leads to a partially reduced surface. The reduced surface can be described electrically as a donor state, since it thermally releases electrons into the conduction band. The oxygen desorption is suppressed for Rh-doped In_2O_3. The corresponding enhancement of the oxidation state of the surface layer prevents an interaction with oxidizing gases like NO_2 due to minimizing accessible electrons required for ionsorption, resulting in a reduced and even suppressed sensitivity, respectively. As a result the sensitivities toward NO_2 can be predicted simply on the base of the materials resistance in reference atmosphere.

At the same time sensitivities toward reducing gases decrease with temperature. Rhodium is known to be one of the most active doping elements for the oxygen activation oxide supported metals catalysts due to its activity in spillover oxygen to the oxide support.[23,24] A similar explanation involving oxygen spillover was given for high resistances observed for Cu doped SnO_2 films.[25] Therefore we assume that the observed property changes due to doping are related with the spillover of oxygen.

The correlations described in this work where discovered only through the multitude of the data under investigation and the associated statistical reliability. Therefore the use of the high-throughput screening HTIS represents a valuable tool for the research in the filed of gas sensing materials as well as generaly in the field of the investigation of electrical properties of solid materials. Accompanied with the obvious acceleration in material preselection, systematic trends as well as structure−property relations are accessible by means of statistical techniques, like data mining.

Acknowledgment. This work was funded by the German Federal Ministry of Education and Research (BMBF) (FKZ03C0305) as well as the Robert Bosch GmbH, Germany.

References and Notes

(1) Gurlo, A.; Ivanovskaya, M.; Pfau, A.; Weimar, U.; Göpel, W. *Thin Solid Films* **1997**, *307*, 288−293.
(2) Cantalini, C.; Wlodarski, W.; Sun, H. T.; Atashbar, M. Z.; Passacantando, M.; Phani, A. R.; Santucci, S. *Thin Solid Films* **1999**, *350*, 276−282.
(3) Steffes, H.; Imawan, C.; Fricke, P.; Vöhse, H.; Albrecht, J.; Schneider, R.; Stolzbacher, F.; Obermeier, E. *Sens. Actuators B* **2001**, (1−2), 352−358.
(4) Steffes, H.; Imawan, C.; Stolzbacher, F.; Obermeier, E. *Sens. Actuators B* **2001**, *78*, 106−112.
(5) Bogdanov, P.; Ivanovskaya, M.; Comini, E.; Faglia, G.; Sberveglieri, G. *Sens. Actuators B* **1999**, *57*, 153−158.
(6) Belysheva, T. V.; Kazachkov, E. A.; Gutman, E. E. *J. Anal. Chem.* **2001**, *59* (7), 676−678.
(7) Chung, W.-Y. *J. Mater. Sci. Lett.* **2002**, *22*, 907−909.
(8) Epifani, M.; Capone, S.; Rella, R.; Siciliano, P.; Vasanelli, L. *J. Sol-Gel Sci. Technol.* **2003**, *26*, 741−744.
(9) Kalinina, M. V.; Tikhonov, P. A.; Nakusov, A. T. *Glass Phys. Chem.* **2003**, *29* (6), 626−631.
(10) Manno, D.; Micocci, G.; Serra, A.; Di Guilo, M.; Tepore, A. *J. Appl. Phys.* **2000**, *88* (11), 6571−6577.
(11) Korotcenkov, G.; Brinzari, V.; Cerneavschi, A.; Ivanov, M.; Cornet, A.; Morante, J.; Cabot, A.; Arbiol, J. *Sens. Actuators B* **2004**, *98*, 122−129.
(12) Ivanovskaya, M.; Kotsikau, D.; Faglia, G.; Nelli, P.; Irkaev, S. *Sens. Actuators B* **2003**, *93*, 422−430.
(13) Barsan, N.; Schweizer-Berberich, M.; Göpel, W. *Fresenius J. Anal. Chem.* **1999**, *365*, 287−304.
(14) Simon, U.; Sanders, D.; Jockel, J.; Heppel, C.; Brinz, T. *J. Comb. Chem.* **2002**, *4* (5), 511−515.
(15) Simon, U.; Sanders, D.; Jockel, J.; Brinz, T. *J. Comb. Chem.* **2005**, *7* (5), 682−687.
(16) Frantzen, A.; Scheidtmann, J.; Frenzer, G.; Maier, W. F.; Jockel, J.; Brinz, T.; Sanders, D.; Simon, U. *Angew. Chem., Int. Ed.* **2004**, *43* (6), 752−754.
(17) Siemons, M.; Simon, U. *Sens. Actuators B* **2006**, *120*, 110−118.
(18) Marezio, M. *Acta Crystallogr.* **1967**, *1*, 1948−2953: *Accra* **1966**, *20*, 723−728.
(19) Barsan, N.; Weimar, U. *J. Electroceram.* **2001**, *7*, 143−167.
(20) Franke, M. E.; Koplin, T. J. Simon, U. *Small* **2006**, *2* (1), 36−50.
(21) Weiher, R. L.; Ley, R. P. *J. Appl. Phys* **1966**, *37*, 299
(22) Christou, V.; Etchells, M.; Renault, O.; Dobson, P. J.; Salata, O. V.; Beamson, G.; Egdell, R. G. *J. Appl. Phys.* **2000**, *88*, 5180
(23) Martin, D.; Duprez, D. *J. Phys. Chem.* **1996**, *100*, 9429−9438.
(24) Descorme, C.; Duprez, D. *Appl. Catal. A* **2000**, *202*, 231−241.
(25) Korotcenkov, G.; Macsanov, V.; Brinzari, V.; Tolstoy, V.; Schwank, J.; Cornet, A.; Morante, J. *Thin Solid Films* **2004**, *467*, 209−214.

CC060044P